A&A 506, 689–702 (2009)
DOI: 10.1051/0004-6361/200811586

Astronomy & Astrophysics

CI and CO in nearby galaxy centers

The star-burst galaxies NGC 278, NGC 660, NGC 3628, NGC 4631, and NGC 4666

F. P. Israel

Sterrewacht Leiden, Leiden University, PO Box 9513, 2300 RA Leiden, The Netherlands
e-mail: israel@strw.leidenuniv.nl

Received 23 December 2008 / Accepted 15 August 2009

ABSTRACT

Aims. We study the physical properties and mass of molecular gas in the central regions of galaxies with active nuclei.

Methods. Maps and measurements of the J = 1–0, J = 2–1, J = 3–2, J = 4–3 ^{12}CO, the J = 1–0, J = 2–1 and J = 3–2 ^{13}CO lines in the central arcminute squared of NGC 278, NGC 660, NGC 3628, NGC 4631, and NGC 4666, as well as 492 GHz [CI] maps in three of these are used to model the molecular gas.

Results. All five objects contain bright CO emission in the central regions. Clear central concentrations were found in NGC 660, NGC 3628, and NGC 4666, but not in the weakest CO emitters NGC 278 and NGC 4631. In all cases, the observed lines could be modeled only with at least two distinct gas components. The physical condition of the molecular gas is found to differ from galaxy to galaxy. Relatively tenuous (density 100–1000 cm^{-3}) and high kinetic temperature (100–150 K) gas occur in all galaxies, except perhaps NGC 3628, mixed with cooler (10–30 K) and denser (0.3–1.0 × 10^4 cm^{-3}) gas. The CO-to-H_2 conversion factor X is typically an order of magnitude less than the "standard" value in the Solar Neighborhood in all galaxy centers. The molecular gas is constrained within radii between 0.6 and 1.5 kpc from the nuclei. Within these radii, H_2 masses are typically 0.6–1.5 × 10^8 $M_\odot$, which corresponds to no more than a few per cent of the dynamical mass in the same region.

Key words. galaxies: ISM – submillimeter – galaxies: nuclei – galaxies: starburst – galaxies: spiral

1. Introduction

Molecular hydrogen (H_2) is a major constituent of the interstellar medium in late-type galaxies. Dense clouds of molecular gas are commonly found in the arms of spiral galaxies, but are frequently also concentrated in the inner few kiloparsecs. These concentrations of gas play an important role in the evolution of galaxy centers. They provide the material for the occurrence of inner galaxy star-bursts and the accretion of super-massive black holes in the nucleus. It is therefore important to determine their characteristics (density, temperature, excitation) and especially their mass but molecular hydrogen itself is very hard to observe directly. Instead, its properties are usually inferred from observations of tracer elements, notably the relatively abundant and easily excited CO molecule. Unfortunately, the CO emitting gas is not in LTE, and the most commonly observed ^{12}CO lines are optically thick. We have to observe CO in various transitions to obtain reliable physical results and also in an optically thin isotope such as ^{13}CO in order to break the temperature-density degeneracy that plagues ^{12}CO intensities. The measured molecular (and atomic) line intensities are the essential input for modeling of the physical state of the gas.

We have observed a sample of nearby spiral galaxy centers in various CO transitions and in the 492 GHz ^{3}P$_1$–^{3}P$_0$ [CI] transition. These galaxies were selected to be bright at infrared wavelengths, and more specifically to have IRAS flux densities $f_{12\,\mu m} \geq 1.0$ Jy. The results for a dozen galaxies from this sample have already been published. These are NGC 253 (Israel et al. 1995), NGC 7331 (Israel & Baas 1999), NGC 6946 and M 83 = NGC 5236 (Israel & Baas 2001 – Paper I), IC 342 and Maffei 2 (Israel & Baas 2003 – Paper II), M 51 = NGC 5194 (Israel et al. 2006 – Paper III), NGC 1068, NGC 2146, NGC 3079, NGC 4826, and NGC 7469 (Israel 2009 – Paper IV). In this paper, we present the results obtained for five bright galaxies undergoing intense star formation (star-burst) in their inner parts. We have summarized basic observational parameters of these galaxies in Table 1.

Although the appearance of all five galaxies in this paper is completely dominated by a central star-burst, NGC 4666 and perhaps NGC 3628 also contain a very modest AGN. NGC 660 shows clear evidence for a recent merger event, and NGC 278 may also have experienced a recent (minor) merger. The other three galaxies, NGC 3628, NGC 4631, and NGC 4666, are all interacting with nearby companions. All five galaxies are at similar distances: three of them at about 12 Mpc, one (NGC 4631) somewhat closer at 8 Mpc, and one (NGC 4666) somewhat more distant at 23 Mpc. Thus, our best angular resolutions of 10″–14″ correspond to linear resolutions of typically 600–850 pc. This is not sufficient to reveal appreciable structural detail in the central CO distributions; millimeter array observations are required for that. However, the multi-transition observations of ^{12}CO and ^{13}CO presented here allow us to characterize the overall physical condition of the central molecular gas in ways not possible otherwise.

2. Sample galaxies

2.1. NGC 278 = DDO 9

This is an isolated, relatively small and almost face-on galaxy with a bright nucleus and multiple, spiral arms. Its optical size is about 2′ corresponding to a diameter of 7 kpc. However, in

Table 1. Galaxy parameters.

	NGC 278	NGC 660	NGC 3628	NGC 4631	NGC 4666
Type[a]	SAB(rs)b	SB(s)a pec; HII/Liner	SAb pec sp Liner	SB(s)d	SABc: Liner
RA (B1950)[a]	$00^h49^m14.6^s$	$01^h40^m21.7^s$	$11^h17^m40.3^s$	$12^h39^m41.9^s$	$12^h42^m34.8^s$
Dec (B1950)[a]	+47°16′44″	+13°23′37″	+13°51′49″	+32°48′56″	−00°11′19″
RA (J2000)[a]	$00^h52^m04.3^s$	$01^h43^m02.4^s$	$11^h20^m17.0^s$	$12^h42^m08.0^s$	$12^h45^m08.6^s$
Dec (J2000)[a]	+47°33′02″	+13°38′42″	+13°35′23″	+32°32′29″	−00°27′43″
$V^b_{\rm LSR}$	+630 km s^{-1}	+841 km s^{-1}	+838 km s^{-1}	+618 km s^{-1}	+1523 km s^{-1}
Inclination i^b	28°	70°	87°	86°	70°
Position angle P^b	116°	45°	102°	86°	225°
Distance $D^{a,c}$	12.1 Mpc	13.0 Mpc	11.9 Mpc	7.7 Mpc	22.6 Mpc
Scale	58 pc/″	63 pc/″	58 pc/″	37 pc/″	109 pc/″

Notes: [a] NED, [b] Nishiyama & Nakai. (2000); van Driel et al. (1995); Irwin & Sofue (1996); Rand (2000); Walter, et al. (2004), [c] Moustakas & Kennicutt (2006).

HI its diameter is five times greater (Knapen et al. 2004). Its dust-rich central parts are quite bright not only in the Hα line, but also in the infrared continuum (Dale et al. 2000; Sanders et al. 2003) and the [CII] line (Malhotra et al. 2001) consistent with intense star-forming activity (Ho et al. 1995; Eskridge et al. 2002). Optical images show a bright, compact nucleus, but there is no indication for even a low-luminosity AGN (Tzanavaris & Georgantopoulos 2007). Although NGC 278 has been included in many recent surveys, the only specific study of this galaxy is the one by Knapen et al. (2004), who concluded that its appearance most likely reflects a recent minor merger. Radio mapping yields a total flux density $S_{1.4\,\rm GHz}$ = 0.13 Jy, a source extent of 48″ × 42″ and a non-thermal spectral index $\alpha = -0.66$ (Condon 1983; Condon et al. 1996, $S_\nu \propto \nu^\alpha$). The high-resolution 1.5 GHz map by Condon (1983) shows diffuse emission, various discrete features following the spiral arms, but no radio counterpart to the nucleus. NGC 278 was detected in the $J = 1{-}0$ and $J = 2{-}1$ ^{12}CO transitions by Braine et al. (1993, IRAM, 23″ and 12″) and in the former by Elfhag et al. (1996, Onsala, 33″) and Young et al. (1995, FCRAO) whose 45″ beam was barely sufficient to resolve the galaxy. $J = 3{-}2$ ^{12}CO maps were published by Wielebinski et al. (1999) and again by Dumke et al. (2001, HHT, 24″) who briefly discussed the CO properties of the galaxy.

2.2. NGC 660

NGC 660 is a remarkable galaxy seen mostly edge-on but exhibiting clear merger signs such as out-of-the-plane ("polar ring") tidal features and two intersecting dust lanes. It is one of the two major members of the NGC 628 Group. Radio continuum maps (Condon, 1980; Condon et al. 1982, 1990) reveal an extended radio source with two distinct peaks, separated by 3″ (projected linear separation 190 pc). The apparent dimensions of the radio source vary with beam-size, but a size of 25″ × 12″ (1500 × 800 pc) is a reasonable approximation. Flux densities are $S_{1.5\,\rm GHz}$ = 374 mJy, $S_{4.9\,\rm GHz}$ = 156 mJy for the extended source total whereas the peaks have $S_{4.9\,\rm GHz}$ = 53 and 41 mJy respectively. The radio continuum spectrum is dominated by non-thermal emission but the relatively shallow spectrum ($\alpha = -0.6$) suggests a non-negligible amount of thermal emission from this LINER galaxy. Indeed, high-density ionized gas is implied by the H92α radio recombination line emission detected by Phookun et al. (1998). High-frequency (15 GHz) radio continuum maps reveal several compact continuum sources most likely large complexes of high-density star-forming regions and a compact nuclear source is lacking at radio wavelengths (Carral et al. 1990) nor is there any obvious X-ray counterpart to the nucleus (Dudik et al. 2005). A detailed study of the galaxy, including HI and $J = 1{-}0$, $J = 2{-}1$ ^{12}CO mapping (Nobeyama, 17″, IRAM, 12″) was carried out by Van Driel et al. (1995). The authors concluded that NGC 660 is the result of a merger of two equally massive objects a few billion years ago. Single dish $J = 1{-}0$ ^{12}CO measurements towards the center of NGC 660 have been summarized by Elfhag et al. (1996) and a $J = 1{-}0$ major axis map was presented by Young et al. (1995, FCRAO, 45″). Aalto et al. (1995) measured ^{12}CO and ^{13}CO in the two lower transitions but there appear to be no high-resolution array maps of the CO emission in this galaxy. Strong absorption towards the nucleus of NGC 660 has been detected in HI and in OH by Baan et al. (1992), as well as in H_2CO (cf. Mangum et al. 2008). An outflow was identified by Baan et al. (1992).

2.3. NGC 3628

This is an edge-on Sbc galaxy and part of a close group called the Leo Triplet (Arp 317) which also includes NGC 3627 and NGC 3623. In this paper, we adopt a distance of 11.9 Mpc, which is considerably greater than 6.7 Mpc often found in the literature. Where appropriate, we have recalculated dimensions quoted in other papers for the new distance value. NGC 3628 is a galaxy well-studied in various ways. Its highly disturbed HI distribution betrays its intense interaction with NGC 3627 (Rots 1978; Haynes et al. 1979). Radio continuum observations by Hummel (1980), Condon et al. (1982, 1990), Condon (1987), and Reuter et al. (1991) show an extended central radio core of size 6″ × 1″ (350 × 60 pc) and flux density $S_{1.5\,\rm GHz}$ = 0.2 Jy with a predominantly non-thermal spectrum ($\alpha = -0.86$). OH and HI absorption observations led Schmelz et al. (1987a,b) to propose the existence of a small, rapidly rotating circumnuclear disk with an outer radius of 365 pc, i.e. nearly twice the size of the radio continuum central disk. As in NGC 660, formaldehyde is seen in absorption against the extended central radio continuum source suggesting the presence of large masses of high-density molecular gas (Mangum et al. 2008, and references therein). Indeed, the center of NGC 3628 resembles that of NGC 660 also by its complement of compact radio continuum sources (none coinciding with the nucleus) representing active regions in the circumnuclear star-burst contributing about 10% to the total radio continuum emission (Carral et al. 1990), and by its H92α radio recombination line emission from high-density HII regions ($n_{\rm HII} \approx 10^4$ cm^{-3} – Anantharamaiah et al. 1993; Zhao et al. 1997). The central core of NGC 3628 is also bright in X-rays, and the galaxy has an extended halo of soft X-ray emission surrounding a central outflow, apparently a galactic (star-burst-driven) super-wind bubble (Dahlem et al. 1996, 1998; Strickland et al. 2004a,b; Grimes et al. 2005; Flohic et al. 2006). NGC 3628 may (Roberts et al. 2001; González-Martín et al. 2006) or may not (Dudik et al. 2005) contain a low-luminosity AGN.

Single dish $J = 1{-}0$ ^{12}CO observations have been reported by Rickard et al. (1982, NRAO, 55″), Young et al. (1983, FCRAO, 45″), and Braine et al. (1993, IRAM, 22″; $J = 2{-}1$, 12″, as well). Higher-resolution (10″–20″) ^{12}CO maps were published by Boissé et al. (1987, IRAM, $J = 1{-}0$, 22″), Israel et al. (1990, JCMT, $J = 2{-}1$, 21″), Reuter et al. (1991, IRAM, $J = 2{-}1$, 12″); major-axis maps of ^{12}CO and ^{13}CO in the $J = 1{-}0$ transition were presented by Praline et al. (2001, FCRAO, 45″). NGC 3628 was also mapped in the $J = 1{-}0$ ^{12}CO transition at high resolutions (3.85″) with the Nobeyama array (Irwin & Sofue 1996).

2.4. NGC 4631

NGC 4631 is an edge-on spiral galaxy interacting with another edge-on spiral neighbor, NGC 4656, and possibly also with the dwarf elliptical NGC 4627 (cf. Combes 1978). The distribution of HI throughout the group has been mapped by e.g. Welsher et al. (1978) and Rand (1994); the WSRT providing a 12″ × 22″ beam very similar to the resolution of our CO measurements. Both total-intensity and major-axis-velocity maps show strong warping and corrugation of the galaxy disk. Notwithstanding its edge-on orientation, many star formation regions are seen in Hα (Crillon & Monnet 1969) and UV (Smith et al. 2001), which are evidently located at the nearby edge of the galaxy. Radio continuum maps (De Bruyn 1977; Condon 1983; Goal 1999) as well as (sub)millimeter and far-infrared maps (Braine et al. 1995; Dumke et al. 2003; Bendo et al. 2006) show the inner 3′ to be even brighter at these wavelengths, suggesting the occurrence of a major star-burst within $R \leq 2.5$ kpc, with the possibility of a "ring" at $R = 30''$, or 1.1 kpc. However, no emission from the nucleus has been identified. The galaxy does have a non-thermal halo (Ekers& Sancisi 1977).

In addition to significant emission from out-of-the plane hydrogen and dust, the structure of the large diffuse X-ray halo together with the observed radio structures suggests wind-driven outflow from a mild star-burst in the central 5 kpc of the disk (Wang et al. 2001; Strickland 2004a,b). However, the lack of a central concentration in star formation is remarkable. In this sense, NGC 4631 resembles NGC 278 more than the other galaxies in this paper.

The major axis of NGC 4631 has been mapped in $J = 1{-}0$ ^{12}CO and ^{13}CO by Young et al. (1995) and Paglione et al. (2001), both using the FCRAO telescope with a resolution of 45″, and in the $J = 2{-}1$ ^{12}CO transition by Sofue et al. (1990, IRAM, 13″). The galaxy was fully mapped in the $J = 1{-}0$ and $J = 2{-}1$ transitions of ^{12}CO by Golla & Wielebinski (1994, IRAM, 22″ and 12″), who also observed ^{13}CO at five different positions in the same transition. They found that CO emission extends over 7′ (15 kpc) along the plane of NGC 4631, but mostly occur within a diameter of 2′ (4.5 kpc), corresponding to the star-burst region delineated in radio and X-ray emission. However, CO is not concentrated to the center. A map of NGC 4631 in $J = 3{-}2$ ^{12}CO was published by Dumke et al. (2001), who also noted the similarities between NGC 278 and NGC 4631. Finally, the inner 100″ (3700 pc) of the galaxy were mapped at high resolution in $J = 1{-}0$ ^{12}CO by Rand (2000, BIMA, 10″ × 7″), who identified a molecular component in the outflow from the center as well as extended CO structure in the disk itself.

2.5. NGC 4666

The IRAS survey revealed the highly tilted Sc galaxy NGC 4666 to be an infrared-luminous star-forming galaxy part of a small group of galaxies also containing NGC 4668 and NGC 4632 (García 1993; see also Walter et al. 2004). In the last decade or so, the galaxy has been observed frequently as part of various surveys, but few detailed studies exist. In the first of these, Dahlem et al. (1997) found that the central 5.5 kpc (reduced to our adopted distance of 22.6 Mpc) of NGC 4666 is the host of a star-burst from which a galactic super-wind flows out into an extended halo. Star-burst, outflow and halo can be identified in X-rays (Dahlem et al. 1997, 1998; Persic et al. 2004). In addition to a star-burst, NGC 4666 also hosts a modest AGN (Persic et al. 2004; Dudik et al. 2005). NGC 4666 thus presents an appearance similar to that of the much closer NGC 3079 (see Israel 2009, and references therein). Low resolution (VLA) radio continuum maps have been presented by Condon (1983), Condon et al. (1990), and Dahlem et al. (1997) who found integrated flux-densities of about 0.16 Jy at 4.9 GHz and 0.40 Jy at 1.5 GHz. No nuclear (point source) flux density has been determined so far; from Condon et al. (1990) an upper limit is $S_{1.5} \leq 0.17$ Jy must be assumed. A major-axis map of NGC 4666 in $J = 1{-}0$ ^{12}CO was published by Young et al. (1995, FCRAO, 45″). Maps in HI and in the $J = 1{-}0$ ^{12}CO (SEST: 45″, IRAM 21″, OVRO 4″ × 3″) as well as the $J = 2{-}1$ ^{12}CO (IRAM: 11″) transitions were published by Walter et al. (2004). These authors found direct evidence for interactions within the group, probably causing the star-burst in NGC 4666.

3. Observations and reduction

The observations described in this paper were carried out with the 15 m James Clerk Maxwell Telescope (JCMT) on Mauna Kea (Hawaii)[1] and with the IRAM 30 m telescope in Pico Veleta (Spain)[2].

3.1. JCMT observations

At the epoch of the mapping observations (1991–2001) the absolute pointing of the telescope was good to about 3″ rms as provided by pointing observations with the JCMT submillimeter bolometer. The spectra were calibrated in units of antenna temperature $T_{\rm A}^{*}$, correcting for sideband gains, atmospheric emission in both sidebands and telescope efficiency. Calibration was regularly checked by observation of a standard line source. Further observational details are given in Tables 2 and 3. Most of the observations were carried out with the now defunct receivers A2, B3i and C2. Observations in 2001 were obtained with the newer receivers B3 (330/345 GHz) and W/C (461 GHz). Full details on these receivers can be found at the JCMT website (`http://docs.jach.hawaii.edu/JCMT/HET/GUIDE/`). Up to 1993, we used a 2048-channel AOS backend covering a band of 500 MHz (650 km s^{-1} at 230 GHz).

[1] The James Clerk Maxwell Telescope is operated on a joint basis between the United Kingdom Particle Physics and Astrophysics Council (PPARC), the Netherlands Organisation for Scientific Research (NWO) and the National Research Council of Canada (NRC).

[2] The IRAM 30 m telescope is supported by INSU/CNRS (France), MPG (Germany), and IGN (Spain).

Table 2. ^{12}CO observations Log.

Galaxy	Date	T_{sys} (K)	Beam size (″)	η_{mb}	t(int) (s)	Map parameters No. pnts	Size (″)	Spacing (″)	PA (°)
J = 1–0 (115 GHz)									
NGC 278	05Nov.	375	22	0.74	2400	1	–	–	–
NGC 660	05Feb.	233			600	1	–	–	–
NGC 3628	05Oct.	305			1200	1	–	–	–
NGC 4631	06Jul.	220			780	1	–	–	–
NGC 4666	06Jul.	293			840	1	–	–	–
J = 2–1 (230 GHz)									
NGC 278	05Nov.	554	12	0.53	960	1	–	–	–
	91Nov./01Sep.	950/315	21	0.69	600/300	36	60 × 40	10	0
NGC 660	05Feb.	250	12	0.53	360	1	–	–	–
91Sep./02Jan.	1040/602	21	0.69	300/600	30	40 × 70	10	51	
NGC 3628	05Oct.	357	12	0.53	1200	1	–	–	–
	89Feb.	1335	21	0.72	1200	29	70 × 50	10	105
NGC 4631	06Jul.	343	12	0.53	780	1	–	–	–
	91Apr./01May.	772/302	21	0.70	400/300	53	120 × 40	10	84
NGC 4666	06Jul.	224	12	0.53	840	1	–	–	–
	00Dec./01Nov.	1104/325	21	0.69	300/480	70	60 × 130	10	0
J = 3–2 (345 GHz)									
NGC 278	00Jul./01Jan.	625/440	14	0.63	240/480	45	50 × 50	8	0
NGC 660	95Jul./00Jul.	1039/701		0.61	960/1080	29	30 × 70	10	51
NGC 3628	94Apr./94Nov.	534/870		0.58	240/400	50	120 × 40	8	105
NGC 4631	01Nov.	485		0.63	240	47	80 × 40	8	84
NGC 4666	00Feb./00Jul.	517/441		0.63	900/2700	48	70 × 70	6	0
J = 4–3 (461 GHz)									
NGC 278	01Jan.	1370	11	0.53	600	11	12 × 18	6	0
NGC 660	99Aug.	3900		0.53	2400	8	18 × 18	6	51
NGC 3628	94Apr.	2716		0.50	720	15	36 × 24	6	105
NGC 4631	96Apr.	1679		0.50	2400	5	24 × 24	6	86
NGC 4666	01Nov.	2785		0.52	1440	13	24 × 24	6	0

After that year, the DAS digital autocorrelator system was used in bands of 500 and 750 MHz. Integration times (on+off) given in Tables 2 and 3 are typical values appropriate to the maps. We subtracted second order baselines from the profiles. All spectra were scaled to a main-beam brightness temperature, $T_{mb} = T_A^*/\eta_{mb}$; values of η_{mb} used are listed in Tables 2 and 3.

All maps were made in rectangular grids (parameters given in Table 2), rotated to parallel the major axis of the galaxy mapped. The maps shown in this paper all have been rotated back to a regular grid in right ascension and declination.

3.1.1. IRAM observations

Observations of both ^{12}CO and ^{13}CO in the J = 1–0 and J = 2–1 transitions at resolutions of 21″ and 12″ respectively were obtained towards the centers of all galaxies with the IRAM 30 m telescope in the period 2005–2007. We used the IRAM facility low-noise receivers A and B in both the 3 mm and the 1 mm bands. For back-ends we used the 1 MHz and 4 MHz filter banks, as well as the VESPA correlator. Initially, all four transitions were observed simultaneously, therefore with identical pointings. After this, the signal-to-noise ratio of the ^{13}CO profiles was increased by additional simultaneous observation of the two transitions, where we took care to ensure that the pointing was the same as for the earlier observations. Calibration and reduction procedures were standard and similar to those described in the previous section. The assumed η_{mb} values are likewise given in Tables 2 and 3. The IRAM observations were especially important not only because they provide measurements of the 3 mm J = 1–0 transitions not possible with the JCMT. The IRAM aperture is twice that of the JCMT, so that the combination of the two data sets provides $J = -1/J$ = 1–0 and J = 3–2/J = 2–1 ratios in closely-matched beams.

3.2. Results

Central line profiles in all observed transitions are shown in Figs. 1 through 5. We mapped the distribution of the molecular gas in the galaxy centers in the J = 2–1, J = 3–2, and J = 4–3 transitions, typically over an area of about one arcminute across. These maps are also shown in the figures, as are the major-axis position-velocity diagrams of the central CO emission.

Measured line intensities towards the center of each galaxy are listed in Table 4. This Table contains entries both at full resolution, and at resolutions corresponding to those of transitions observed in larger beams. These entries were extracted from maps convolved to the resolution quoted. The convolution was carried out with the map interpolation function of the SPECX data reduction package[3]. This function interpolates, where necessary, the map intensities by using adjacent pixels out to a preset distance (usually 2 beams) and convolved the observed and interpolated data points with a two-dimensional Gaussian function ("beam") of predetermined half-width. This half-width is chosen such that the actual observing beam convolved with the 2D-Gaussian would yield a beam corresponding to the desired resolution. Velocities in a position-velocity map can also be "smoothed" by applying a convolving Gaussian function in a similar manner.

[3] http://docs.jach.hawaii.edu/JCMT/cs/005/11/html/node129.html

Table 3. ^{13}CO and [CI] observations Log.

Galaxy	Date	T_{sys} (K)	Beam ($''$)	η_{mb}	t(int) (s)
J = 1–0 (110 GHz)					
NGC 278	05Nov.	147	23	0.75	2220
NGC 660	05Feb.	130			780
NGC 3628	05Oct.	162			1200
NGC 4631	06Jul.	150			1560
NGC 4666	06Jul.	189			2520
J = 2–1 (220 GHz)					
NGC 278	95Jun.	678	22	0.69	4730
	05Nov.	283	13	0.55	2040
NGC 660	01May	351	22	0.69	1800
	05Feb.	259	13	0.55	780
NGC 3628	95Jun.	324	22	0.69	3000
	05Oct.	212	13	0.55	1320
NGC 4631	01Mar.	444	22	0.69	1800
	06Jul.	260	13	0.55	1560
NGC 4666	00Dec.	520	22	0.69	3600
	06Jul.	498	13	0.55	2520
J = 3–2 (330 GHz)					
NGC 278	01Jan.	567	14	0.63	6600
NGC 660	01Jan.	653		0.61	4800
NGC 3628	94Apr.	1129		0.58	4800
NGC 4631	02jun.	895		0.63	4800
NGC 4666	04Feb.	1073		0.63	36000
CI $^3P_1 - ^3P_0$					
J = 1–0 (492 GHz)					
NGC 278	96Jul.	3640	11	0.53	1800
NGC 660	96Jul.	3063		0.50	1800
NGC 3628[a]	94Nov.	3421		0.50	1440

Note: [a] Small map of 8 points, size $18'' \times 18''$, spacing $6''$, in PA 114°.

Finally, we have determined the line intensity ratios of the observed transitions at the center of the galaxies observed. They have been determined independently from the intensities given in Table 4. Specifically: (a) we used data taken at the same observing run wherever possible, (b) we determined ratios at various resolutions convolving the maps to the relevant beam widths, and (c) we verified ratios by comparing profile shapes in addition to integrated intensities. In Table 5, whenever data were insufficient for convolution, or altogether lacking (e.g. [CI]), no entry is provided.

4. Analysis

4.1. Radiative transfer modelling of CO

We have modeled the observed ^{12}CO and ^{13}CO line intensities and ratios with the large-velocity gradient (LVG) radiative transfer models described by Jansen (1995) and Jansen et al. (1994) – but see also Hogerheijde & van der Tak (2000) and the web page `http://www.strw.leidenuniv.nl/~michiel/ratran/`. These codes provide model line intensities as a function of three input parameters per molecular gas component: gas kinetic temperature T_k, molecular hydrogen density $n(H_2)$ and the CO column density per unit velocity $N(CO)/dV$. Full details of the relevant molecular and atomic line data used in these models can be found in Schöier et al. (2005). By comparing model to observed line *ratios*, we may identify the physical parameters best describing the actual conditions at the observed positions. Beam-averaged properties are determined by comparing observed and model *intensities*. In principle, with seven measured line intensities of two isotopes, properties of a single gas component are overdetermined as only five independent observables are required. In practice, this is mitigated by degeneracies such as occur for ^{12}CO. In any case, we find that fits based on a single-component gas are almost always incapable of fully matching the data.

However, we usually obtain good fits based on *two* gas components. The solutions for a two-component gas are slightly under-determined but we can successfully compensate for this by introducing additional constraints as described below. The physical gas almost certainly has a much larger range of temperatures and densities but with the present data two components is the maximum that can be considered. Indeed, adding even one more component increases the number of free parameters to the point where solutions are physically meaningless. Thus, our two-component model gas is only an approximation

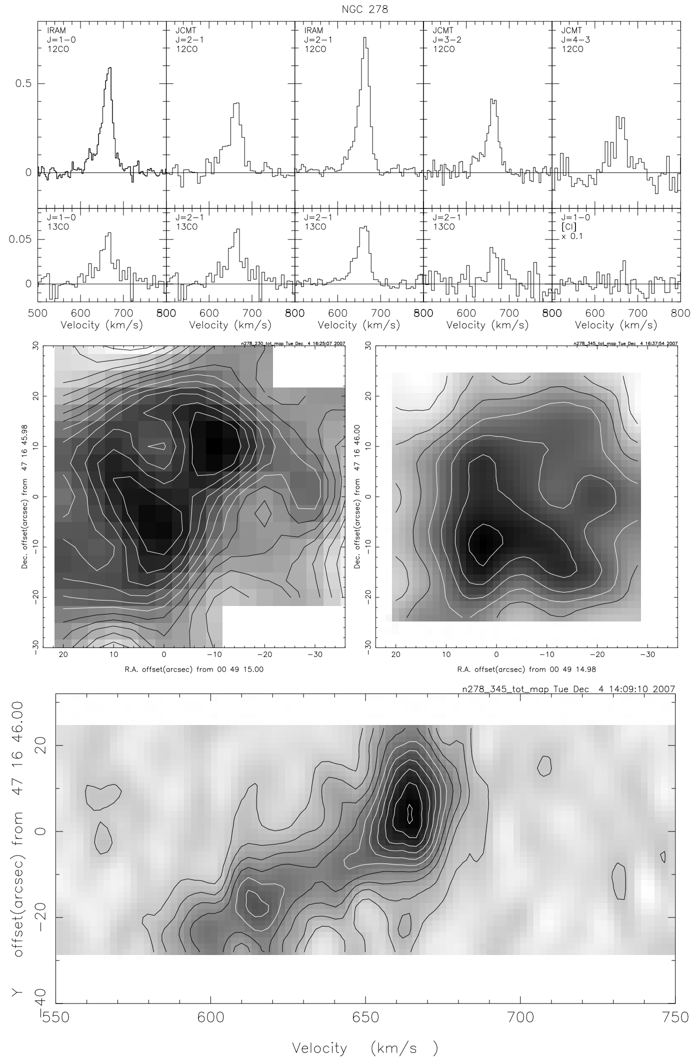

Fig. 1. CO in the center of NGC 278. *Top*: observed line profiles. Horizontal scale is LSR velocity V_{LSR} in km s^{-1}. Vertical scale is main-beam brightness temperature T_{mb} in Kelvins, using the efficiencies listed in Table 2. Note different scales for ^{12}CO, ^{13}CO and [CI] respectively. *Center*: (*left*) J = 2–1 ^{12}CO emission integrated over the velocity interval 550–750 km s^{-1}. Contours are in steps of 1 K km s^{-1}; here and in all other figures, the first contour is equal to the step value; (*right*) J = 3–2 ^{12}CO emission integrated over the same velocity interval; contour step is 2 K km s^{-1}. *Bottom*: J = 3–2 ^{12}CO; position-velocity map in position angle PA = 45° integrated over a strip 20$''$ wide with contours in steps of 0.04 K; northeast is at top.

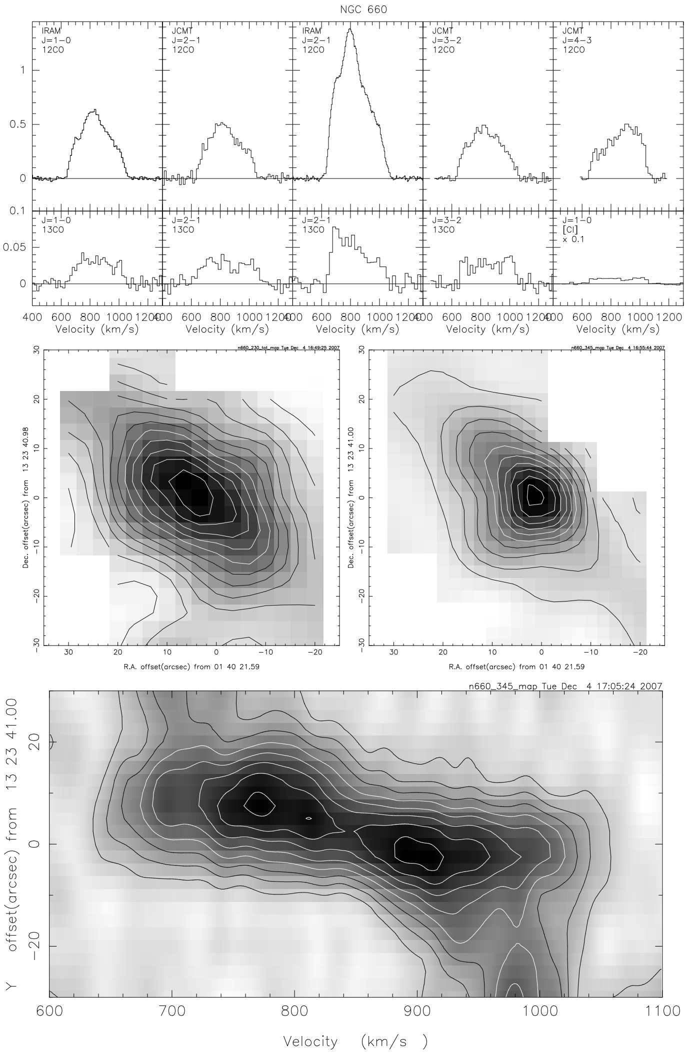

Fig. 2. Center of NGC 660, as Fig. 1. *Top*: observed line profiles. *Center*: (*left*) J = 2−1 ^{12}CO emission integrated over the velocity interval 600–1100 km s^{-1}; contour step is 10 K km s^{-1}; (*right*) J = 3−2 ^{12}CO emission integrated over the same velocity interval; contour step is 15 K km s^{-1}. *Bottom*: J = 3−2 ^{12}CO; position-velocity map in position angle PA = 51° integrated over a strip 20″ wide with contours in steps of 0.04 K; northeast is at top.

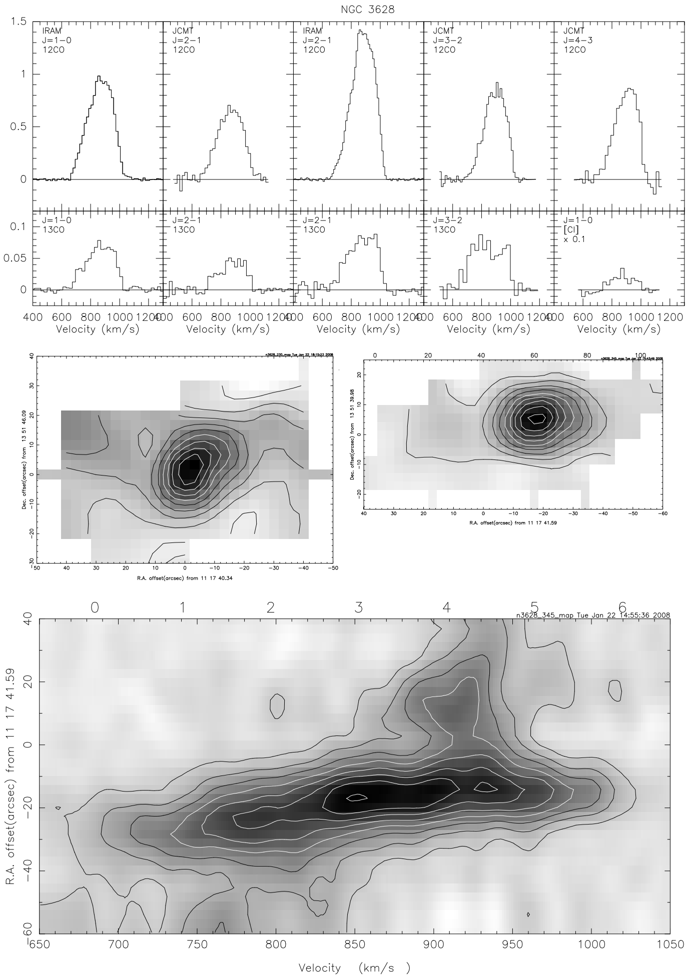

Fig. 3. Center of NGC 3628, as Fig. 1. *Top*: observed line profiles. *Center*: (*left*) J = 2−1 ^{12}CO emission integrated over the velocity interval 650–1050 km s^{-1}; contour step is 15 K km s^{-1}; (*right*) J = 3−2 ^{12}CO emission integrated over the same velocity interval; contour step is 20 K km s^{-1}. *Bottom*: J = 3−2 ^{12}CO; position-velocity map in position angle PA = 120° integrated over a strip 20″ wide with contours in steps of 70 mK; east is at top.

of reality but it is decidedly superior to one-component model solutions. As long as significant fractions of the total molecular gas mass are limited to similar segments of parameter space, they also provide a reasonably realistic model for the actual state of affairs. Specifically, our analysis is less sensitive to the occurrence of gas at very high densities and temperatures, but such gas is unlikely to contribute significantly to the total mass.

In order to reduce the number of free parameters, we assumed identical CO isotopic abundances for both gas components. Furthermore, in a small number of star-burst galaxy centers (NGC 253, NGC 4945, M 82, IC 342, He 2-10), values of 40 ± 10 have been suggested for the isotopic abundance [^{12}CO]/[^{13}CO] (Mauersberger & Henkel 1993; Henkel et al. 1993, 1994, 1998; Bayet et al. 2004), somewhat higher than the characteristic value of 20–25 for the Milky Way nuclear region (Wilson & Rood 1994). We therefore have adopted an abundance value of [^{12}CO]/[^{13}CO] = 40 in our models. We identified acceptable fits by searching a grid of model parameter combinations (10 K ≤ T_k ≤ 150 K, 10^2 cm^{-3} ≤ $n(H_2)$ ≤ 10^5 cm^{-3}, 6×10^{15} cm^{-2} ≤ $N(CO)/dV$ ≤ 3×10^{18} cm^{-2}) for model line ratios matching the observed set, with the relative contribution of the two components as a free parameter. The models rarely predict the precise set of line ratios that is observed. The ^{12}CO ratios are generally derived from observations taken at different times, and require convolution of one of the lines to the resolution of the other. In contrast, ^{12}CO/^{13}CO line ratios are derived from observations done (quasi)simultaneously and in with identical beams, so that they are much more accurately determined. Thus, when confronted with competing sets of model ratios in which one or more of the individual ratios differs from the observed ratio beyond the observational uncertainty, we value a good fit to the ^{12}CO transition ratios much less than one to the observed ^{12}CO/^{13}CO line ratios. Comparison of the entries in Table 5 and the last six columns of Table 6 shows that this choice had to be made for NGC 3628 (in particular for the J = 4−3/J = 2−1 ratio, and also for NGC 4631 which is difficult to fit with any model set.

Solutions obtained in this way are not unique, but rather define a limited range of values in distinct regions of parameter space. For instance, variations in input parameters may to some extent compensate one another, producing identical line

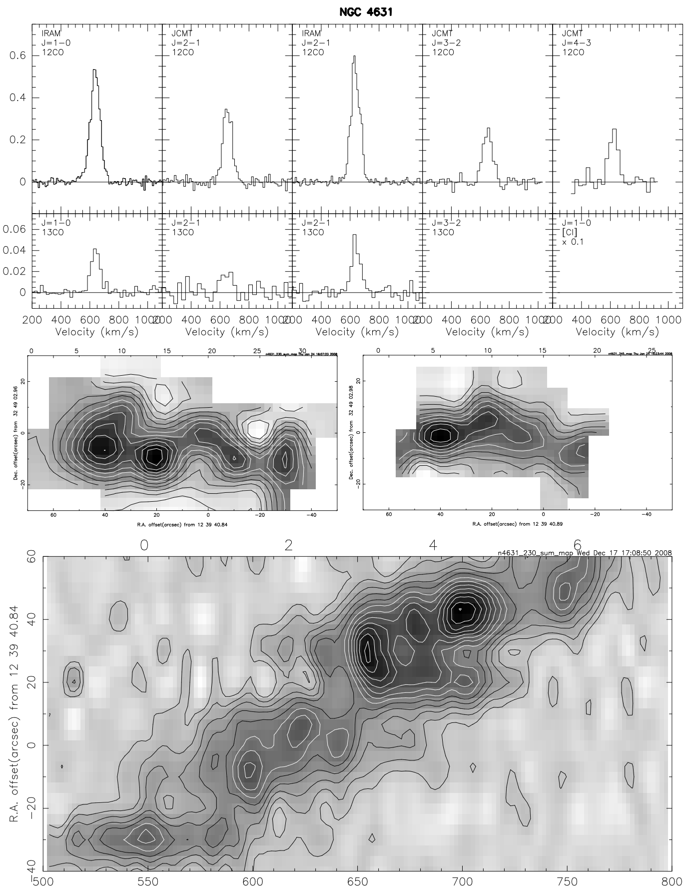

Fig. 4. Center of NGC 4631, as Fig. 1. *Top*: observed line profiles. *Center*: (*left*) $J = 2{-}1$ ^{12}CO emission integrated over the velocity interval 500–800 km s^{-1}; contour step is 4 K km s^{-1}; (*right*) $J = 3{-}2$ ^{12}CO emission integrated over the same velocity interval; contour step is 4 K km s^{-1}. *Bottom*: $J = 2{-}1$ ^{12}CO; position-velocity map in position angle PA = 94° integrated over a strip 20″ wide with contours in steps of 40 mK; east is at top.

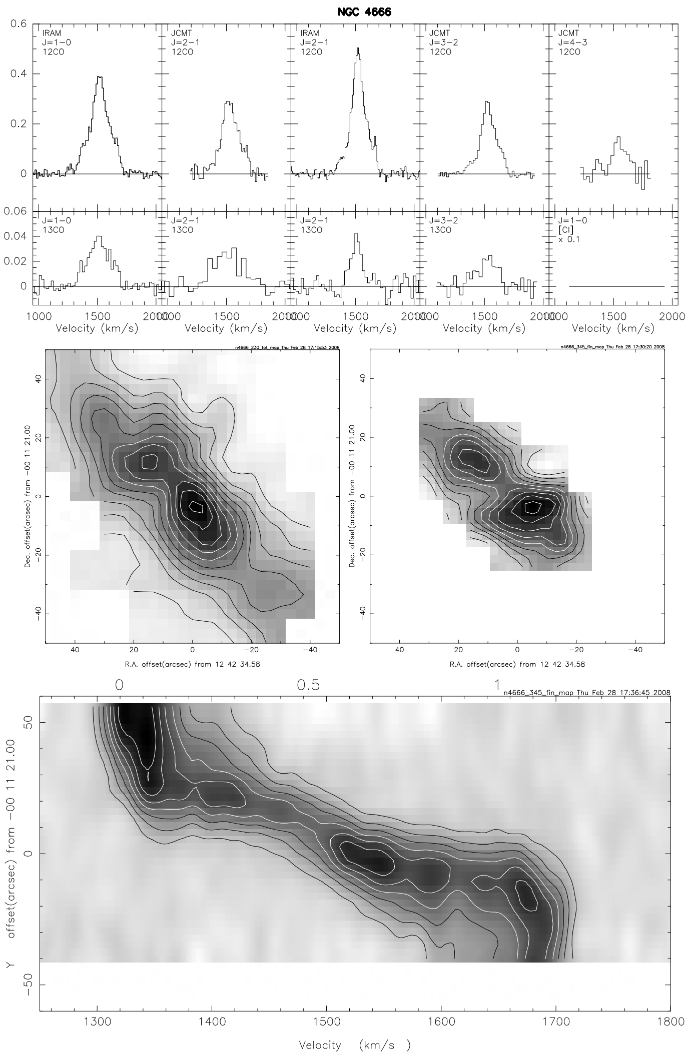

Fig. 5. Center of NGC 4666, as Fig. 1. *Top*: observed line profiles. *Center*: (*left*) $J = 2{-}1$ ^{12}CO emission integrated over the velocity interval 1250–1800 km s^{-1}; contour step is 5 K km s^{-1}; (*right*) $J = 3{-}2$ ^{12}CO emission integrated over the same velocity interval; contour step is 5 K km s^{-1}. *Bottom*: $J = 3{-}2$ ^{12}CO; position-velocity map in position angle PA = 45° integrated over a strip 20″ wide with contours in steps of 15 mK; east is at top.

ratios for somewhat different combinations of input parameters. Among all possible solution sets, we have rejected those in which the denser gas component is also much hotter than the more tenuous component, because we consider the large pressure imbalances implied by such solutions physically implausible, certainly on the kilo-parsec scales observed.

The results of our model fitting procedure are summarized in Table 6. The table lists, under the proviso just given, representative model solutions reproducing the observed line ratios. In appropriate cases (e.g. N 278, N 660, and N 3628), two solutions are given, each representative of a group of solutions with very similar parameters. No galaxy observation set yielded more than two groups of plausible solutions. The Table gives for each of the two representative gas components the kinetic temperature $T_{\rm kin}$, the H_2 volume density $n\,H_2$, and the CO gradient $\frac{N({\rm CO})}{{\rm d}V}$. The relative contribution of the two components to the observed $J = 2{-}1$ ^{12}CO emission is also given. The last six columns give the corresponding model ratios, which may be compared directly to the observed ratios (in a 21″ beam) in Table 5.

4.2. Beam-averaged molecular gas properties

Chemical models, such as presented those by van Dishoeck & Black (1988) and recently updated by Visser et al. (2009), show a strong dependence of the (neutral and ionized) atomic carbon to carbon monoxide column density ratio, N(C)/N(CO), on the total carbon $N_{\rm C} = N({\rm C}) + N({\rm CO})$ and molecular hydrogen column densities. With line intensities $I_{\rm CO}$, $I_{\rm [CI]}$, and $I_{\rm [CII]}$ of all three species known, minimal assumptions suffice to deduce total carbon and hydrogen column densities and masses.

Unfortunately, when we have *incomplete or no knowledge* of these C° and C$^+$ line intensities, as is the case here and often elsewhere as well, this procedure is useless. However, lacking direct and full atomic carbon information, we may still make progress by using a new element instead. The total [C]/[H] gas-phase carbon abundance may serve equally well as a constraining factor in addition to the CO column density resulting from the radiative transfer model. The chemical models provide the fraction of CO (i.e. the ratio of carbon monoxide to atomic carbon, whether neutral or ionized) as a function of H_2 column density. The fraction derived from the models varies as a function of H_2 volume density and the radiation field. In all cases we used the H_2 density derived from the LVG modeling. For the *average* radiation field, we assumed relatively moderate conditions to apply

Table 4. Measured central ^{12}CO and ^{13}CO line intensities.

	Beam size ($''$)	NGC 278 $T_{\rm mb}$ (mK)	NGC 278 $\int T_{\rm mb} dV$ (K km s^{-1})	NGC 660 $T_{\rm mb}$ (mK)	NGC 660 $\int T_{\rm mb} dV$ (K km s^{-1})	NGC 3628 $T_{\rm mb}$ (mK)	NGC 3628 $\int T_{\rm mb} dV$ (K km s^{-1})	NGC 4631 $T_{\rm mb}$ (mK)	NGC 4631 $\int T_{\rm mb} dV$ (K km s^{-1})	NGC 4666 $T_{\rm mb}$ (mK)	NGC 4666 $\int T_{\rm mb} dV$ (K km s^{-1})
^{12}CO											
J = 1–0	22	595	21 ± 2	635	163 ± 16	980	211 ± 25	550	45 ± 6	395	77 ± 9
J = 2–1	12	755	26 ± 3	1377	352 ± 35	1420	207 ± 25	600	45 ± 6	505	74 ± 9
	21	393	16 ± 2	516	137 ± 14	710	151 ± 18	390	26 ± 3	320	54 ± 6
	43	—	14 ± 2	—	62 ± 8	—	71 ± 9	—	21 ± 3	—	27 ± 3
J = 3–2	14	414	15 ± 2	490	164 ± 19	860	163 ± 20	280	22 ± 3	315	51 ± 6
	21	—	13 ± 2	—	94 ± 11	—	130 ± 15	—	17 ± 2	—	37 ± 4
J = 4–3	11	310	15 ± 2	565	161 ± 16	930	176 ± 21	250	19 ± 2	150	28 ± 5
	14	—	11 ± 1	—	122 ± 14	—	140 ± 17	—	14 ± 2	—	23 ± 3
	21	—	9 ± 1	—	92 ± 11	—	98 ± 12	—	—	—	16 ± 2
^{13}CO											
J = 1–0	21	68	2.5 ± 0.3	34	10.4 ± 1	72	17.1 ± 2.0	40	3.45 ± 0.38	40	8.8 ± 1.0
J = 2–1	12	64	2.7 ± 0.3	66	18.7 ± 2	82	20.9 ± 2.5	60	3.75 ± 0.45	40	11.3 ± 1.3
	21	77	1.9 ± 0.3	44	11.4 ± 1	46	13.6 ± 1.7	20	1.20 ± 0.14	30	8.1 ± 0.8
J = 3–2	14	55	1.3 ± 0.2	32	12.9 ± 1	77	20.6 ± 2.5	—	—	25	4.5 ± 0.6

Table 5. Adopted velocity-integrated line ratios in galaxy centres.

Transitions	Beam ($''$)	NGC 278	NGC 660	NGC 3628	NGC 4631	NGC 4666
^{12}CO						
(1–0)/(2–1)	21	0.89 ± 0.16	1.19 ± 0.17	1.40 ± 0.28	1.72 ± 0.26	1.42 ± 0.21
(2–1)/(2–1)	12/21	1.58 ± 0.24	2.57 ± 0.40	1.38 ± 0.28	1.68 ± 0.25	1.37 ± 0.21
(3–2)/(2–1)	21	0.79 ± 0.13	0.69 ± 0.11	0.62 ± 0.12	0.66 ± 0.10	0.69 ± 0.10
(3–2)/(2–1)	12	0.74 ± 0.13	0.66 ± 0.12	0.87 ± 0.17	0.58 ± 0.09	0.80 ± 0.12
(4–3)/(2–1)	21	0.56 ± 0.08	0.66 ± 0.11	0.65 ± 0.13	—	0.30 ± 0.05
(4–3)/(2–1)	12	0.54 ± 0.10	0.49 ± 0.09	0.74 ± 0.15	0.46 ± 0.07	0.36 ± 0.05
^{12}CO/^{13}CO						
(1–0)	21	8.4 ± 1.3	15.7 ± 2.0	12.2 ± 1.8	13.0 ± 2.0	8.5 ± 1.3
(2–1)	21	8.6 ± 1.4	12.2 ± 1.8	11.7 ± 1.6	22.2 ± 3.3	6.7 ± 1.0
(2–1)	12	9.6 ± 1.5	18.8 ± 2.8	13.2 ± 1.9	11.4 ± 1.6	6.3 ± 1.0
(3–2)	14	11.4 ± 1.7	12.8 ± 1.9	7.9 ± 1.8	—	11.3 ± 1.7
[CI]/CO(2–1))	21	0.29 ± 0.04	0.20 ± 0.05	0.28 ± 0.06	—	—

Table 6. Radiative transfer model parameters.

No.	Component 1 Kin. temp. $T_{\rm k}$ (K)	Component 1 Gas dens. $n({\rm H_2})$ (cm^{-3})	Component 1 Gradient $\frac{N({\rm CO})}{dV}$ ($\frac{\rm cm^{-2}}{\rm km\,s^{-1}}$)	Component 2 Kin. temp. $T_{\rm k}$ (K)	Component 2 Gas dens. $n({\rm H_2})$ (cm^{-3})	Component 2 Gradient $\frac{N({\rm CO})}{dV}$ 1:2 ($\frac{\rm cm^{-2}}{\rm km\,s^{-1}}$)	Emiss. ratio Comp. 1:2	Model ratios ^{12}CO $\frac{(1-0)}{(2-1)}$	^{12}CO $\frac{(3-2)}{(2-1}$	^{12}CO $\frac{(4-3)}{(2-1)}$	^{12}CO/^{13}CO (1–0)	^{12}CO/^{13}CO (2–1)	^{12}CO/^{13}CO (3–2)
NGC 278													
1	100	500	10×10^{17}	30	10 000	0.3×10^{17}	3:17	0.92	0.79	0.52	8.0	8.9	11.0
2	150	100	30×10^{17}	30	10 000	0.3×10^{17}	1:4	0.94	0.80	0.53	8.2	9.2	11.5
NGC 660													
3	150	500	0.6×10^{17}	20	100 000	0.3×10^{17}	11:9	1.17	0.75	0.49	15.8	11.8	12.9
4	150	100	0.6×10^{17}	150	3000	1.0×10^{17}	4:1	1.17	0.72	0.50	16.3	12.3	12.1
NGC 3628													
5	150	1000	3.0×10^{17}	20	10 000	0.3×10^{17}	1:9	1.10	0.74	0.43	12.8	12.2	8.9
6	20	100	1.0×10^{17}	30	10 000	0.6×10^{17}	17:3	1.32	0.63	0.47	12.4	12.3	8.7
NGC 4631													
7	150	1000	1.0×10^{17}	10	300	0.45×10^{17}	1:5	1.52	0.65	0.42	13.5	10.5	13.2
NGC 4666													
8	100	1000	1.0×10^{17}	10	10 000	0.6×10^{17}	7:13	1.32	0.70	0.37	8.5	6.7	11.7

to the objects studied here, e.g. radiation field intensities typically about an order of magnitude higher than those in the Solar Neighborhood, or less. At the same time, the gas phase carbon abundance provides us with the total carbon column (i.e. the sum of carbon monoxide and atomic carbon) for any H2 column density. Thus, each value of $N({\rm H_2})$ is associated with a unique value of N(C)/N(CO) *and* a unique value of $N_{\rm C} = N({\rm C}) + N({\rm CO})$. Knowing any one of the three column densities (e.g. N(CO), the two equations allow us to find the remaining columns (e.g. $N({\rm H_2})$ and (C)). What fraction of all atomic carbon (C) is ionized (C^+) or neutral (C°) remains undetermined, but that does not concern us here.

Oxygen abundances and gradients of many nearby galaxies have been compiled by Vila-Costas & Edmunds (1992), Zaritsky et al. (1994), and Pilyugin et al. (2004). None of the five galaxies studied here is included in any of these compilations. The first two compilations suggest nuclear metalicities many times solar, but Pilyugin et al.'s more recent work implies nuclear metalicities on average only 1.5 times solar. A major uncertainty in these values is caused by the extrapolation of disk HII region abundances to the very different galaxy center environment. We have conservatively assumed a metalicity twice solar for the galaxy central regions. The results published by Garnett et al. (1999) suggest very similar carbon and oxygen abundances at these metalicities, so that we adopt [C]/[H] $\approx$ 1.0 $\times$ 10^{-3}. As a significant fraction of carbon is tied up in dust particles and thus unavailable in the gas-phase, we have also adopted a fractional correction factor $\delta_c = 0.27$ (see for instance van Dishoeck & Black 1988), so that $N_H/N_C = [2N(H_2) + N(HI)]/[N(CO) + N(CII) + N(CI)] = 3700$, uncertain by about a factor of two. In Table 7 we present beam-averaged column densities for CO and C (=C°+C$^+$), as well as H_2 derived under these assumptions. As the observed peak CO intensities are significantly below the model peak intensities, only a small fraction of the (large) beam surface area can be filled with emitting material.

Although the analysis in terms of two gas components is superior to that assuming a single component, it is not fully realistic. For instance, the assumption of e.g. *identical beam filling factors* for the various species (^{12}CO, ^{13}CO, C°, and C$^+$) is not a priori plausible. However, as argued before (cf. Israel 2009), the beam-averaged column-density is modified only by the degree of non-linearity in the response of the model parameters to a change in filling factor, *not* by the magnitude of that change. A similar state of affairs exists with respect to *model degeneracy*. Even for rather different model fractions of hot or dense gas, in any particular galaxy the *beam-averaged* molecular hydrogen densities are practically the same. The uncertainties introduced by plausibly different average radiation fields are also relatively minor. As we are observing with a large linear beamsize, we are not sensitive to the very highly excited or very dense molecular gas that only occurs on small scales. In fact, the assumed gas-phase carbon abundance dominates the results.

The derived beam-averaged column-densities (and projected mass densities) roughly scale inversely proportional to the square root of the abundance assumed: $N_{av} \propto [C]/[H]_{gas}{}^{-0.5}$. As our estimate of the central elemental carbon abundance, and our estimate of the carbon depletion factor are unlikely to be wrong by more than a factor of two, the resulting uncertainty in the final values listed in Table 7 should be no more than 50%.

5. Discussion

5.1. NGC 278

The CO distribution shown in Fig. 1 reveals that there is no concentration of molecular gas towards the nucleus of the galaxy, as was already suggested by the lower-resolution map of Dumke et al. (2001). Instead, a few local peaks in the extended diffuse emission occur near positions of enhanced radio continuum emission in the spiral arms (see Condon 1986).

This is particularly clear in a map of peak rather than integrated brightness temperature (see Fig. 6), showing unresolved maxima with T_{mb} = 0.5–0.7 K. These CO and radio continuum peaks mark the locations of major star-forming complexes in the inner disk. The molecular gas in the SE arm appears to be somewhat warmer than that in the NW arm. The inner rotation

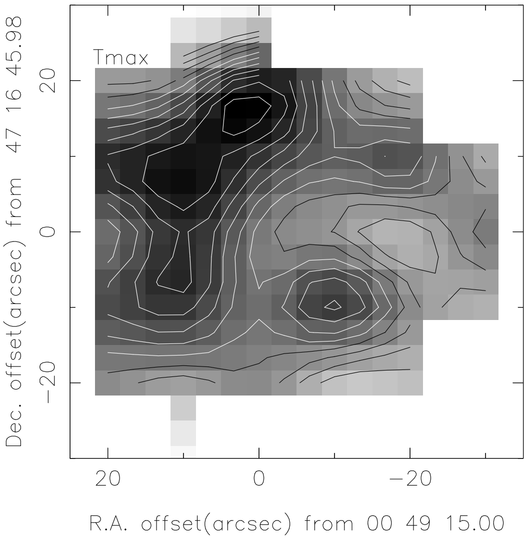

Fig. 6. Center of NGC 278. Map of peak J = 2–1 ^{12}CO brightness temperature T_{mb}. Contour step is 30 mK, lowest contour is at 300 mK.

gradient in Fig. 1 is 150 km s^{-1}/′. Taking into account distance and inclination of the galaxy as listed in Table 1, this corresponds to 90 km s^{-1} kpc^{-1}. The maximum rotational velocity width is 110 km s^{-1}, or 235 km s^{-1} corrected for inclination. In the center of the galaxy, the slow decrease of ^{12}CO intensity with increasing rotational transition (Table 6) suggests the presence of a fair amount of warm molecular gas. At the same time, the ^{13}CO/ ^{12}CO isotope intensity ratios are not particularly high, implying that reasonably dense gas should also be present. Indeed, a robust result of our modeling (Tables 6, 7) is that almost 90 per cent of the molecular gas mass is relatively dense ($n_{H_2} \approx 10^4$ cm^{-3}) and not very warm with a kinetic temperature of about 30 K. The remaining 10 per cent of the molecular mass is much hotter (T_k = 100−150 K) and much less dense (n_{H_2} = 100−500 cm^{-3}). Such temperatures and densities are not unusual for photon-dominated regions (PDRs) associated with the star formation process. Notwithstanding the uncertainty in the hot component parameters, the beam-averaged parameters allow for very little variation. Most of the carbon should be in CO, the ratio of C to CO being 0.4.

The implied face-on molecular hydrogen mass density of 8 $M_\odot$/pc^2 is not exceptional. The relatively low beam-averaged molecular hydrogen column density $N(H_2) = 6 \times 10^{20}$ cm^{-2} combined with the modest J = 1–0 ^{12}CO intensity of 21 K km s^{-1} implies a low value for the CO-to- H_2 conversion factor $X = 3 \times 10^{19}$ cm^{-2}/ K km s^{-1}, i.e. typically 6–7 times less than the Solar Neighbourhood conversion factor. Again, this is not unusual and in line with findings for other galaxies (cf. the discussion in Israel 2009).

5.2. NGC 660

As Fig. 2 shows, there is a clear CO maximum spanning the central (deconvolved) 17″, which means that there is a very significant molecular gas concentration within a radius R = 500 pc from the nucleus. At lower levels of surface brightness, CO emission is present over the full extent of our maps. Indeed, in the (IRAM 30 m) ^{12}CO maps published by Van Driel et al. (1995), ever weaker emission is seen to extend out to radii of 70″ (4.4 kpc). The central CO emission peak in NGC 660 is quite strong (Table 4). The major-axis/velocity diagram suggests

Table 7. Beam-averaged model parameters.

Galaxy		Beam-averaged column densities			Outer radius	Central H_2 mass	Face-on mass density	Relative mass
		N(CO)	N(C)	$N(\mathrm{H_2})$	R	$M_{\mathrm{H_2}}$	$\sigma(\mathrm{H_2})$	component 1:2
		(10^{18} cm^{-2})		(10^{21} cm^{-2})	(kpc)	(10^8 $M_\odot$)	($M_\odot$/pc^{-2})	
NGC 278	1/2	0.24	0.09	0.6	—	—	8	0.90:0.10
NGC 660	3	0.33	0.38	1.3	0.9	0.6	7	0.67:0.33
	4	0.49	0.96	2.7	0.9	1.2	15	0.75:0.25
NGC 3628	5	2.7	0.13	5.2	0.6	1.5	—	0.25:0.75
	6	2.1	0.65	5.1	0.6	1.5	—	0.90:0.10
NGC 4631	7	0.22	0.51	1.4	—	—	—	0.20:0.80
NGC 4666	8	0.30	0.31	1.1	1.5	1.2	6	0.50:0.50

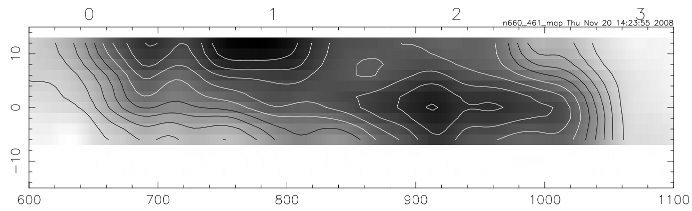

Fig. 7. Center of NGC 660, J = 4–3 ^{12}CO position-velocity map in position angle PA = 45° integrated over a strip 14″ wide with contours in steps of 40 mK; northeast is at top.

that this central molecular gas is in rapid rotation, following a solid-body rotation curve. The velocity gradient of rotation is 355 km s^{-1} kpc^{-1}, corrected for inclination; the full rotational width is 450 km s^{-1}, again corrected for inclination. In Figs. 2 and 7, the very central few arcseconds (corresponding to a radius $R \leq 100$ pc) show a pronounced molecular gas minimum. The size of this minimum corresponds closely to the separation of the radio peaks mentioned earlier. The ^{12}CO ratios in Table 5 suggest that the gas within a radius of 6″ ($R \leq 380$ pc) is both cooler (lower ^{12}CO (4–3)/(2–1) ratio) and less optically thick (higher J = 2–1 ^{12}CO/^{13}CO ratio) than that between radii of 11″ and 6″ (R = 380–700 pc). More in general, the observed line ratios may be explained by either of two models. The corresponding reasonably good fits (see Table 6) are virtually indistinguishable notwithstanding the differences in underlying physical conditions. Tables 6 and 7 show that in the first model, two thirds of the gas mass is hot (T_{kin} = 150 K) and tenuous ($n_{\mathrm{H_2}} \approx 500$ cm^{-3}), and the remaining third is cold (T_{kin} = 20 K) and very dense ($n_{\mathrm{H_2}} \approx 10^5$ cm^{-3}). In the second model, essentially all gas is hot (T_{kin} = 150 K), three quarters is very tenuous ($n_{\mathrm{H_2}} \approx 100$ cm^{-3}) and the remaining quarter is only modestly dense ($n_{\mathrm{H_2}} \approx 3000$ cm^{-3}). Overall, the two models lead to integrated central masses and projected mass densities different by a factor two, the latter model yielding the highest values. As either of the two solutions yields plausible parameters, it is not easy to determine which model is the more likely to apply. We may nevertheless firmly conclude that in the center of NGC 660 *most of the molecular gas is very hot and rather tenuous*. The corresponding CO-to H_2 conversion factor in the center of is $X = 0.8$–1.6×10^{19} cm^{-2}/ K km s^{-1}, i.e. 12–25 times *lower* than the "standard" Solar Neighborhood value. We find that the implied central gas mass is 1–2% of the dynamical mass in the same volume.

5.3. NGC 3628

Figure 3 shows bright CO emission from the galaxy, strongly concentrated in the inner 30″ (i.e. within radii $R \leq 850$ pc).

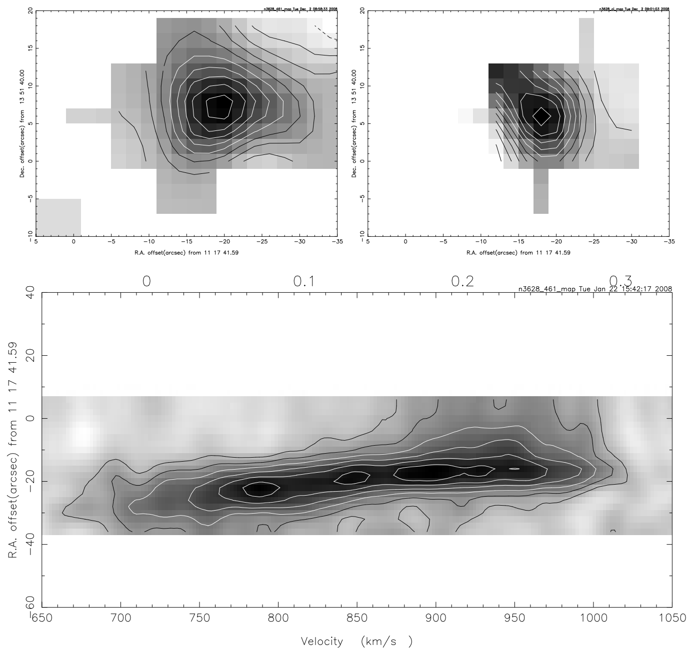

Fig. 8. Center of NGC 3628. *Top*: (*Left*) J = 4–3 ^{12}CO emission integrated over the velocity interval 650–1050 km s^{-1}; contour step is 40 K km s^{-1}; (*right*) [CI] emission integrated over the same velocity interval; contour step is 5 K km s^{-1}, lowest contour is at 20 K km s^{-1}. *Bottom*: J = 4–3 ^{12}CO position-velocity map in position angle PA = 105° integrated over a strip 20″ wide with contours in steps of 10 mK; east is at top.

The overall extent suggested by our J = 3–2 ^{12}CO single-dish measurements is in excellent agreement with the size shown in the J = 1–0 ^{12}CO array map by Irwin & Sofue (1996). The major-axis velocity diagram shows two kinematic components. A fast-rotating feature in the center extends over only half this size. It is superposed on molecular gas in more leisurely rotation extending over the full area mapped in CO. The extent of the fast-rotating component is the same as that of the OH/HI absorption feature measured by Schmelz et al. (1987a,b). The velocity gradient of rotation is 360 km s^{-1} kpc^{-1}, corrected for inclination – very similar to that of NGC 660, but the full rotational width of 305 km s^{-1} (again corrected for inclination) is much less than that of NGC 660. The molecular gas distribution in Figs. 3 and 8 does not exhibit an obvious central minimum such as most other galaxies do but we cannot rule out that the limited spatial resolution and the steep velocity gradient conspire to hide a small central minimum. The IRAM J = 2–1 ^{12}CO maps by Reuter et al. (1991) suggest that this is indeed the case. The fact that the radio core is about half the size of the extent of the molecular gas in the fast-rotating component suggests that much of the star-burst takes place at the inside of this molecular gas concentration. Throughout the central region, we have observed emission from neutral carbon. However, the very center shows an unresolved (i.e. diameter less than 250 pc) [CI] peak (Fig. 8).

The line ratios in Table 5 suggest that the observed molecular gas is only modestly optically thick. Comparison of the ratios in a 21″ beam with those in a 12″ beam implies that the molecular gas in the central region close to the radio core (marking the star-burst) is denser or warmer than the gas at slightly greater (R = 350–600 pc) distances to the nucleus. We suspect that the former is the dominant effect, because almost all the molecular gas in the center of NGC 3628 is relatively cold: all model fits, including those shown in Table 6, solidly suggest predominant temperatures $T_{\rm kin}$ = 20–30 K. In model 5, most of the gas is both cool and dense ($n_{\rm H_2}$ = 10^4 cm^{-3}) but there is a non-negligible mass of hot ($T_{\rm kin}$ = 150 K) and less dense ($n_{\rm H_2}$ = 10^3 cm^{-3}) gas. In model 6, all of the gas is cool, and most of it is rather tenuous ($n_{\rm H_2}$ = 10^2 cm^{-3}). In this model, there is only a small mass of cool gas at higher densities ($n_{\rm H_2}$ = 10^4 cm^{-3}). Given the star-burst nature of NGC 3628, model 5 appears physically more plausible, as is also suggested by the presence of warm dust in NGC 3628 (Rice et al. 1988). In terms of beam-averaged quantities, the difference between the two models is slight. In model 5 almost all (95%) of all carbon is in CO. In model 6 this fraction is somewhat lower (75%). Both have beam-averaged H_2 column densities $N_{\rm H_2}$ ≈ 5×10^{21} cm^{-2} which is very similar to the peak HI column density listed by Braun et al. (2007). These column densities are relatively high but this is not surprising given the edge-on orientation of the galaxy. Because of this, we could not reliably estimate the face-on mass-density. The central molecular gas mass is $M_{\rm H_2}$ = $1.5\times10^8\,M_\odot$ within R = 0.6 kpc, independent of the model assumed. Towards the center of NGC 3628, the CO-to H_2 conversion factor is $X = 2.4 \times 10^{19}$ cm^{-2}/ K km s^{-1}, i.e. 8 times *lower* than the "standard" Solar Neighborhood value. A roughly similar value was also estimated by Irwin & Sofue (1996). The molecular mass in the central region calculated by us is typically 2–6% of the dynamical mass.

5.4. NGC 4631

The CO maps in Fig. 4 are more detailed than those published earlier by Golla & Wielebinski (1994) and Dumke et al. (2001), but similar overall aspect. The maps published by these authors show that the most intense CO emission ranges from $\Delta\alpha = +60'$ to $\Delta\alpha = -40''$ in our map which just covers this range. CO intensities are at a relative minimum at the position of the nucleus of the galaxy, which is located not at the map (0, 0) position, but offsets $\Delta\alpha = +12.5''$, $\Delta\delta = -6''$. In the integrated intensity maps, nor in the major axis-velocity map is there any sign of molecular gas associated with the nucleus, a conclusion we share with Rand (2001). In addition, the velocity-integrated CO brightness temperatures are much lower in NGC 4631 (and NGC 278) than in galaxies with distinct central CO concentrations such as, for instance, NGC 660 and NGC 3628. There are, however, several unresolved CO intensity peaks at various distances to the midplane of the galaxy. These might be thought to reflect spiral arm tangential locations but this is not very probable because they are not placed symmetrically with respect to the nucleus. More likely they are instead giant molecular cloud complexes hosting the burst of star formation that is taking place in the central region of NGC 4631. In support of this, we note that they tend to coincide with radio continuum peaks in the map by Golla (1999),

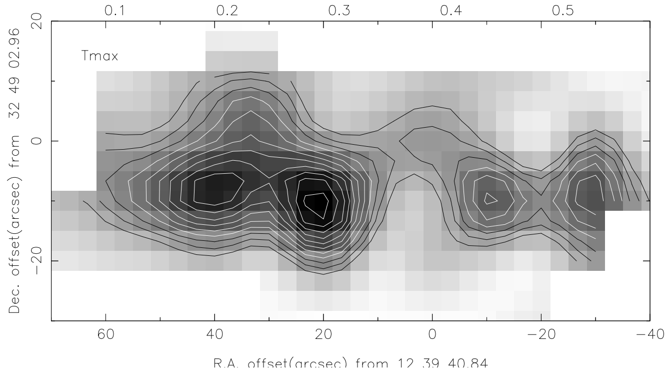

Fig. 9. Center of NGC 4631. Map of peak J = 2−1 ^{12}CO brightness temperature $T_{\rm mb}$. Contour step is 50 mK, lowest contour is at 300 mK.

while the easternmost and brightest CO peak also corresponds to the Hα emission region CM 67 (Crillon & Monnet 1969). The peak CO brightness temperatures in Fig. 9 are $T_{\rm mb}$ = 0.5−0.8 K. These are almost identical to the brightness temperatures found for similar CO peaks in NGC 278 and suggest filling factors of the order of 0.02–0.05 when compared with Galactic GMC's of typical size 100–150 pc. If we could view NGC 4631 face-on, it would probably much resemble NGC 278. Contrary to earlier interpretations, we do not find the observed CO structure of NGC 4631 to suggest the presence of ring- or bar-like structures in the galaxy.

The line ratios of the diffuse gas in the line of sight through the center of NGC 4631 (Table 5) do not allow much choice in model parameters. Twenty per cent of the gas mass sampled in this direction is warm ($T_{\rm kin}$ ≈ 150 K) and moderately dense ($n_{\rm H_2}$ ≈ 1000 cm^{-3}) but most (80%) of it is cold ($T_{\rm kin}$ ≈ 10 K) and relatively tenuous ($n_{\rm H_2}$ ≈ 300 cm^{-3}). In this particular direction which does not sample an active center nor an actively star forming region, beam-averaged H_2 column densities are not particularly high (cf. Table 7) and most (70%) of the carbon appears to be in atomic form. Towards the center of NGC 4631 we find a CO-to H_2 conversion factor $X = 3.1\times10^{19}$ cm^{-2}/ K km s^{-1}, i.e. 6 times *lower* than the "standard" Solar Neighborhood value. Paglione et al. (2001) estimated an X-factor only slightly higher than this towards the center of NGC 4631. Thus, the implied molecular gas mass in NGC 4631 is much lower, and a much smaller fraction of the dynamical mass, than use of the "standard" conversion factor would suggest.

5.5. NGC 4666

The maps in Fig. 5 show CO emission to extend over 120″ (13 kpc) in the plane of the galaxy. This extent only marginally exceeds that of the CO emission mapped at high resolution by Walter et al. (2004, their Fig. 8). The ^{12}CO maps show a strong central peak, which we also observed in the J = 4−3 transition (Fig. 10). Although the slightly asymmetrical CO distribution in our J = 3−2 ^{12}CO position-velocity map suggests a small offset from the nucleus, this central CO peak is in fact coincident with the kinematic center of the galaxy derived from the HI emission by Walter et al. (2004). Nevertheless, their CO array maps show that the central molecular gas maximum seen in our maps in the lower J transitions is, in fact, a blend of a compact CO maximum centered on the nucleus and star-forming molecular clouds in the disk close to the nucleus. The compact appearance of the central

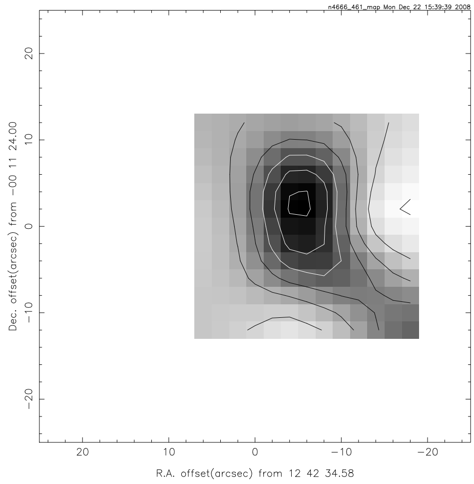

Fig. 10. Center of NGC 4666. Map of velocity-integrated J = 4–3 ^{12}CO brightness temperature $T_{\rm mb}{\rm d}V$. Contour step is 1.5 K km s^{-1}, lowest contour is at 3 kkms

condensation in the J = 4–3 ^{12}CO map (Fig. 10) implies that it is significantly denser than the gas farther from the nucleus.

The inner parts of NGC 4666 rotate fast, with an inclination-corrected velocity span of 360 km s^{-1} over the central arcminute. Unlike most of the other galaxies mapped by us, the inner parts of NGC 4666 do not quite follow a solid-body rotation curve.

We note that the ^{12}CO/^{13}CO ratios of NGC 4666 are relatively low and similar to those of NGC 278. As is the case in that galaxy, such values suggest the relatively high CO optical depths characteristic of star-forming Giant Molecular Clouds in the Milky Way disk. Our model analysis in Tables 6 and 7 yields roughly equal masses of modestly dense ($n_{\rm H_2}$ ≈ 10^3 cm^{-3}) and hot ($T_{\rm kin}$ ≈ 100 K) gas and dense ($n_{\rm H_2}$ ≈ 10^4 cm^{-3}) and cold ($T_{\rm kin}$ ≈ 10 K) gas. There are roughly equal masses of neutral carbon and carbon monoxide. Molecular hydrogen column densities, central mass, and face-on mass density do not stand out with respect to the other galaxies discussed in this paper. The central CO-to-H_2 conversion factor implied by Tables 4 and 7 is only $X = 1.4 \times 10^{19}$ cm^{-2}/ K km s^{-1}, a factor 14 lower than the Solar Neighborhood standard. The central mass is about 0.5 per cent of the dynamical mass.

5.6. Column densities and masses

For the galaxies in this paper, we find H_2 column densities averaged over a 21″ beam of roughly 0.5–5 × 10^{21} cm^{-2} (corresponding to *total hydrogen* columns of 1–10 × 10^{21} cm^{-2}). Thus, these galaxies cover a somewhat greater range than the 2–6 × 10^{21} cm^{-2} that we found for more active galaxies in our previous paper (Israel 2009) and they are mostly somewhat lower. These total columns also include the ambient contribution by neutral atomic hydrogen which we have so far neglected. Previously, we have found that HI *absorption* column densities actually measured usually exceed the *beam-averaged* H_2 column densities we derive. This is also the case for the only two galaxies with HI absorption results in the literature, NGC 660 (Baan et al. 1992) and NGC 3628 (Schmelz et al. (1987a), with typical HI absorption column densities N(HI) ≈ 10^{22} cm^{-2}, i.e. 4–7 the value listed in Table 7 for NGC 660, and twice the value given for NGC 3628. However, the effective absorbing area is smaller by at least an order of magnitude than the large 21″ beam over which we have averaged our H_2 in Table 7. More importantly, in these highly tilted galaxies much of the HI seen in absorption must reside in the disk, and the actual HI content of the central region is unknown (see also the discussion by Baan et al. 1992). Although we have no direct knowledge of central HI column densities in the present sample, we note that most (if not all) galaxies with strong central molecular gas concentrations exhibit a pronounced lack of HI emission at their centers. In the six more or less face-on galaxies previously studied by us, we found a mean value N(HI) = $0.6 \pm 0.3 \times 10^{21}$ cm^{-2}, and there is no reason to assume that the galaxies discussed here are very different. Indeed, in the HI *channel maps* of NGC 4666, there is a clear lack of neutral hydrogen at the position of the nuclear CO peak (Walter et al. 2004, their Fig. 9). From the previous results, we estimate that the HI contribution to the total hydrogen column densities derived by us is small, typically 10 per cent uncertain by a factor two either way. However, the one face-on galaxy discussed here, NGC 278, clearly lacks a central molecular concentration and here the HI contribution may be significant.

The H_2 masses derived are again much lower than those calculated previously by authors who assumed the "standard" CO-to-H_2 conversion factor X to apply. If we were to have underestimated the HI contribution, or to have overestimated the CO column density, these H_2 masses would be even lower. With the results presented for the galaxy centers in this paper, we find X = 0.1–0.3 × 10^{20} cm^{-2}/(K km s^{-1}) which is a factor of 7–20 lower than the 'standard' Milky Way X factors (see also Strong et al. 2004), but quite similar to those found in other galaxy centers (Israel 2009; Israel & Baas 2003, and references therein). We also note that at least for NGC 3628 our present result is practically identical to the low value (X = 0.2–0.7 × 10^{20} cm^{-2}/(K km s^{-1}) found independently by Irwin & Sofue (1996). With the low X values presented here, the molecular gas does not constitute more than typically a few per cent of the total (dynamical) mass in the same volume.

5.7. Temperature and excitation

Although a classical UV-illuminated photon-dominated region (PDR) associated with a star-forming region may reach quite high kinetic temperatures, the mass of gas at such elevated temperatures is rather small and limited to the immediate vicinity of the stellar heating source. Even in intense star-forming regions globally averaged temperatures are unlikely to be in excess of 20–30 K.

When we look at Table 6 we see that only towards the center of the fully edge-on galaxy NGC 3628 the molecular line emission may arise from a gas purely dominated by *star-bursts*. In the other four galaxy centers, a 10–30 K molecular gas component is always accompanied by a much hotter (usually relatively tenuous) component of temperature 100–150 K. In NGC 278 and NGC 660 this hot component contains, in effect, most of the molecular gas mass, in NGC 4666 it is about half, and only in the quiescent center of NGC 4631 it is a small (20%) fraction. Although the galaxies discussed here all have *star-burst-dominated* central regions, they are thus mostly too hot to be excited only by the UV photons from luminous stars. We found a similar result in the preceding paper on five AGN/star-burst galaxies (Israel 2009). There, as is the case here, central star-bursts were seen to produce extended outflows glowing in soft-X-ray emission. Also the galaxies included in this paper support the suggestion that the hot molecular gas component is efficiently heated by the X-rays from these flows (see Meijerink et al. 2006, 2007) rather than by the UV photons from the star-burst.

5.8. Comparison with AGN central CO emission

A brief comparison with the galaxies containing a (modest) AGN, discussed in our previous paper (Israel 2009) shows a number of resemblances and differences. In galaxy centers of either type, we need to fit the observed CO lines with at least two different molecular gas density/temperature components: a hot and tenuous one, and a cooler and dense one. However, we find that the highest densities occur in galaxy centers that have both a star-burst and an AGN. The size of the central molecular gas concentration is similar whether or not an AGN is present, but its mass and column density are on average lower in the star-burst-only than in the combined star-burst/AGN galaxies. CO emission is also weaker in star-burst-only galaxies, which also tend to have lower ^{12}CO/^{13}CO ratios, hence higher average CO optical depths. The *weakest* CO galaxies in the sample (NGC 278 and NGC 4631) are pure star-burst galaxies *without* a significant central CO concentration. Rather, these galaxies confine their star-burst activity to the disk spiral arms. In galaxies of either type, the CO-to-H_2 conversion factors X appropriate to the central region are low – there is no systematic difference. In terms of excitation, both galaxy center types require another mechanism to operate in addition to the UV excitation from PDRs. X-rays from diffuse gas heated by star-burst-driven winds may be the answer. In any case and at least on scales of a few hundred parsecs or more, (modest) AGNs do not seem to leave an unambiguous imprint on the centrally concentrated molecular gas.

6. Conclusions

1. We have observed the centers of five galaxies undergoing significant star-burst activity in the first four transitions of ^{12}CO and the first three transitions of ^{13}CO, and three of them also in the lower transition of [CI].
2. All galaxies were mapped over at least $1' \times 1'$ in the $J = 2{-}1$ and $J = 3{-}2$ transitions and over a smaller area in the $J = 4{-}3$ transition of ^{12}CO.
3. The central line ratios, reduced to a standard $21''$ beam, vary significantly in the sample galaxies. In general, relatively strong $J = 4{-}3$ line emission indicates elevated densities and perhaps temperatures for the molecular gas.
4. ^{12}CO optical depths appear not to be very high. NGC 660, NGC 3628 and NGC 4631 have ^{12}CO/^{13}CO ratios in the range of 11–16. NGC 278 and NGC 4666 have lower isotopic ratios in the range 6–8 suggesting the somewhat higher optical depths reminiscent of extended molecular clouds in the Solar Neighborhood.
5. In NGC 660, NGC 3628, and NGC 4666 molecular gas is present in the form of clearly identifiable central concentrations of outer radius $R = 0.6{-}1.5$ kpc. Such central concentrations are lacking in NGC 278 and NGC 4631. The central concentrations in NGC 660 and NGC 3628 exhibit a local minimum at the nucleus itself.
6. In the central regions of NGC 660, NGC 3628, and NGC 4666, we find moderate H_2 masses of $0.6{-}1.5 \times 10^8\,M_\odot$. These masses are typically about one per cent of the dynamical mass in the same region. The CO-to-H_2 conversion factors X implied by these masses and the observed $J = 1{-}0$ ^{12}CO line intensities is typically an order of magnitude lower than the "standard" Solar Neighborhood X-factor.
7. The molecular gas of all observed galaxies may at least partly be excited by UV-photons from the extended circumnuclear star-burst, but in all galaxies (except perhaps NGC 3628) a significant fraction of the molecular gas must be excited in other ways such as the X-rays seen to emanate from massive wind-driven outflows.

Acknowledgements. I am much indebted to the late Fred Baas, who died suddenly and far too early in 2001, for carefully planning and performing many of the observations described in this paper. I also thank the various JCMT observers who made additional observations in queue mode. Finally, it is always a pleasure to thank the personnel of both the JCMT and the IRAM 30 m telescope for their able and generous support.

References

Anantharamaiah, K. R., Zhao, J.-H., Goss, W. M., van Gorkom, J. H., & Viallefond F. 1993, ApJ, 419, 585
Baan, W. A., Rhoads, J., & Haschick, A. D. 1992, ApJ, 401, 508
Bayet, E., Gerin, M., Phillips, T. G., & Contursi, A. 2004, A&A, 427, 45
Bendo, G. J., Dale, D. A., Draine, B. T., et al. 2006, ApJ, 652, 283
Boissé, P., Casoli, F., & Combes, F. 1987, A&A, 173, 229
Braine, J., Combes, F., Casoli, F., et al. 1993, A&AS, 97, 887
Braine, J., Krugel, E., Sievers, A., & Wielebinski, R. 1995, A&A, 295, L55
Braun, R., Oosterloo, T. A., Morganti, R., Klein, U, & Beck, R. 2007, A&A, 461, 455
Carral, P., Turner, J. L., & Ho, P. T. P. 1990, ApJ, 362, 434
Combes, F. 1978, A&A, 65, 46
Condon, J. J. 1980, ApJ, 242, 894
Condon, J. J. 1983, ApJS, 53. 459
Condon, J. J. 1987, ApJS, 65, 485
Condon, J. J., Condon, M. A., Gisler, G., & Puschell, J. J. 1982, ApJ, 252, 102
Condon, J. J., Helou, G., Sanders, D. B., & Soifer, B. T. 1990, ApJS, 73, 359
Condon, J. J., Helou, G., Sanders, D. B., & Soifer, B. T. 1996, ApJS, 103, 81
Crillon, R., & Monnet, G. 1969, A&A, 2, 1
Dahlem, M., Heckman, T. M., Fabbiano G., Lehnert, M. D., & Gilmore D. 1996, ApJ, 461, 724
Dahlem, M., Petr M. G., Lehnert, M. D., Heckman, T. M., & Ehle M. 1997, A&A, 320, 731
Dahlem, M., Weaver, K. A., & Heckman, T. M. 1998, ApJS, 118, 401
Dale, D. A., Silbermann, N. A., Helou, G., et al. 2000, AJ, 120, 583
De Bruyn, A. G. 1977, A&A, 58, 221
Dudik, R. P., Satyapal, G. M., & Sambruna, R. M. 2005, ApJ, 620, 113
Dumke, M., Nieten, Ch., Thuma, G., Wielebinski, R., & Walsh, W. 2001, A&A, 373, 853
Dumke, M., Krause, M., & Wielebinski, R. 2004, A&A, 414, 475
Ekers R. D., & Sancisi R. 1977, A&A, 54, 973
Elfhag, T., Booth, R. S., Höglund, B., Johansson, L. E. B., & Sandqvist, A. A. 1996, A&AS, 115, 439
Flohic, H. M. L. G., Eracleous, M., Chartas, G., Shields, J. C., & Moran, E. C. 2006, ApJ, 647, 140
Eskridge, P. H., Frogel, J. A., Pogge, R. W., et al. 2002, ApJS, 143, 73
García, A. M. 1993, A&AS, 100, 47
Garnett, D. R., Shields, G. A., Peimbert, M., et al. 1999, ApJ, 513, 168
Golla, G. 1999, A&A, 345, 778
Golla, G., & Wielebinski, R. 1994, A&A, 286, 733
González-Martín, O., Masegosa, J., Márquez, I., Guerrero, M. A., & Dultzin-Hacyan, D. 2006, A&A, 460, 45
Grimes, H. J. P., Heckman, T., Strickland, D., & Ptak, A. 2005, ApJ, 628, 187
Habing, H. J. 1969, Bull. Astron. Inst. Netherlands, 19, 421
Haynes, M. P., Giovanelli, R., & Roberts, M. S. 1979, ApJ, 229, 83
Henkel C., Mauersberger R., Wiklind T., et al. 1993, A&A, 268, L17
Henkel C., Whiteoak J. B., & Mauersberger R. 1994, A&A, 284, 17
Henkel, C., Chin, Y.-N., Mauersberger, R., & Whiteoak, J. B. 1998, A&A, 329, 443
Ho, L. C., Filippenko A. V., & Sargent W. L. W. 1995, ApJS, 98, 477
Hogerheijde, M. R., & Van der Tak, F. F. S. 2000, A&A, 362, 697
Hummel, E. 1980, A&AS, 41, 151
Irwin, J. A., & Sofue, Y. 1996, ApJ, 464, 738
Israel, F. P. 2009, A&A, 493, 525
Israel, F. P., & Baas, F. 1999, A&A, 351, 10
Israel, F. P., & Baas F. 2001, A&A, 371, 433
Israel, F. P., & Baas, F. 2003, A&A, 404, 495
Israel, F. P., Baas, F., & Maloney, P. R. 1990, A&A, 237, 17
Israel, F. P., White G. J., & Baas F. 1995, A&A, 302, 343
Israel, F. P., Tilanus, R. P., & Baas F. 2006, A&A, 445, 907
Jansen, D. J. 1995, Ph.D., Thesis, University of Leiden (NL)
Jansen, D. J., van Dishoeck, E. F., & Black J. H. 1994, A&A, 282, 605

Knapen, J. H., Whyte L. F., de Blok W. J. G., & van der Hulst J. M. 2004, A&A, 423, 481
Malhotra, S., Kaufman, M. J., Hollenbach, D., et al. 2001, ApJ, 561, 766
Mauersberger R., & Henkel C. 1993, Rev. Mod. Astron. 6, 69
Meijerink, R., Spaans, M. C., & Israel, F. P. 2006, ApJ, 650, L103
Meijerink, R., Spaans, M. C., & Israel, F. P. 2007, A&A, 461, 793
Moustakas, J., & Kennicutt, R. C. 2006, ApJS, 164, 81
Nishima, K., & Nakai, N. 2001, PASJ, 53, 713
Paglione, T. A. D., Wall, W. F., Young, J. S., et al. 2001, ApJ, 135, 183
Petitpas G. R., & Wilson C. D. 1998, ApJ, 503, 219
Persic M., Cappi M., Rephaeli Y., et al. 2004, A&A, 427, 35
Phookun, B., Anantharamaiah, K. R., & Goss, W. M. 1998, MNRAS, 295, 156
Pilyugin, L. S., Vílchez, J. M., & Contini, T. 2004, A&A, 425, 849
Rand, R. J. 1994, A&A, 285, 833
Rand, R. J. 2000, ApJ, 535, 663
Reuter, H.-P., Krause, M., Wielebinski, R., & Lesch, H. 1991, A&A, 248, 12
Rickard, L. J., Bania, T. M., & Turner, B. E. 1982, ApJ, 252, 147
Rice, W., Lonsdale, C. J., Soifer, B. T., et al. 1988, ApJS, 68, 91
Roberts, T. P., Schurch, N. J., & Warwick, S. R. 2001, MNRAS, 324, 737
Rots, A. H. 1978, AJ, 83, 219
Sanders, D. B., Mazzarella, J. M., Kim, D.-C., Surace, J. A., & Soifer, B. T. 2003, AJ, 126, 1607
Schmelz, J. T., Baan, W. A., & Haschick, A. D. 1987a, ApJ, 315, 492
Schmelz, J. T., Baan, W. A., & Haschick, A. D. 1987b, ApJ, 320, 145
Schöier, F. L., van der Tak, F. F. S., van Dishoeck, E. F., & Black, J. H. 2005, A&A, 432, 369
Smith, A. M., Collins, N. R., Waller, W. H., et al. 2001, ApJ, 546, 829
Sofue, Y., Handa, T., Golla, G., & Wielebinski, R. 1990, PASJ, 42, 745
Strickland, D. K., Heckman, T. M., Colbert, E. J. M., Hoopes, C. G., & Weaver, K. A. 2004a, ApJ, 606, 829
Strickland, D. K., Heckman, T. M., Colbert, E. J. M., Hoopes, C. G., & Weaver, K. A. 2004b, ApJS, 151, 193
Strong, A. W., Moskalenko, I. V., Reimer, O., Digel, S., & Diehl, R. 2004, A&A, 422, 47
Stutzki, J., Graf, U. U., Honingh, C. E., et al. 1997, ApJ, 477, L33
Tzanavaris, P., & Georgantopoulos, I. 2007, A&A, 468, 129
van Driel, W., Combes F., Casoli, F., et al. 1995, AJ, 109, 942
van Dishoeck, E. F., & Black, J. H. 1988, ApJ, 334, 771
Vila-Costas, M. B., & Edmunds, M. G. 1992, MNRAS, 259, 121
Visser, R., van Dishoeck, E. F., & Black, J. H. 2009, [arXiv:0906.3699]
Walter, F., Dahlem, M., & Lisenfeld, U. 2004, ApJ, 606, 258
Wang, Q. D., Immler, S., Walterbos, R., Lauroesch, J. T., & Breitschwerdt, D. 2001, ApJ, 555, 99
Weliachew, L., Sancisi, R., & Guélin, M. 1978, A&A, 65, 37
White, G. J., Ellison, B., Claude, S., Dent, W. R. F., & Matheson, D. 1994, A&A, 284, L23
Wielebinski, R., Dumke, M., & Nieten, Ch. 1999, A&A, 347, 643
Wilson, T. L., & Rood, R. T. 1994, ARA&A, 32, 191
Young, J. S., Tacconi, L., & Scoville, N. Z. 1983, ApJ, 269, 136
Young, J. S., Xie, S., Tacconi, L., et al. 1995, ApJS, 98, 219
Zaritsky, D., Kennicutt, R. C., & Huchra, J. P. 1994, ApJ, 420, 87